nature medicine

Niemann-Pick disease type C1 is a sphingosine storage disease that causes deregulation of lysosomal calcium

Emyr Lloyd-Evans[1], Anthony J Morgan[1], Xingxuan He[2], David A Smith[1], Elena Elliot-Smith[1], Daniel J Sillence[3], Grant C Churchill[1], Edward H Schuchman[2], Antony Galione[1] & Frances M Platt[1]

Niemann-Pick type C1 (NPC1) disease is a neurodegenerative lysosomal storage disorder caused by mutations in the acidic compartment (which we define as the late endosome and the lysosome) protein, NPC1. The function of NPC1 is unknown, but when it is dysfunctional, sphingosine, glycosphingolipids, sphingomyelin and cholesterol accumulate. We have found that NPC1-mutant cells have a large reduction in the acidic compartment calcium store compared to wild-type cells. Chelating luminal endocytic calcium in normal cells with high-affinity Rhod-dextran induced an NPC disease cellular phenotype. In a drug-induced NPC disease cellular model, sphingosine storage in the acidic compartment led to calcium depletion in these organelles, which then resulted in cholesterol, sphingomyelin and glycosphingolipid storage in these compartments. Sphingosine storage is therefore an initiating factor in NPC1 disease pathogenesis that causes altered calcium homeostasis, leading to the secondary storage of sphingolipids and cholesterol. This unique calcium phenotype represents a new target for therapeutic intervention, as elevation of cytosolic calcium with curcumin normalized NPC1 disease cellular phenotypes and prolonged survival of the NPC1 mouse.

NPC1 disease is an inherited neurodegenerative acidic compartment lipid storage disorder[1] caused by mutations in the *NPC1* gene that encodes a transmembrane protein of the acidic compartment (NPC1). NPC1 has been suggested to facilitate endocytic transport[2], lysosomal cholesterol efflux[3] and fatty acid efflux[4]. A clinically identical disease results from mutations in the *NPC2* gene, which encodes a soluble protein of the acidic compartment[5]. Currently, the function of NPC1 is unknown, whereas NPC2 is proposed to transport cholesterol from inner lysosomal vesicles to the limiting membrane of the lysosome[6].

An unusual feature of NPC disease is the broad range of lipids that accumulate, including sphingomyelin[7], cholesterol, glycosphingolipids (GSLs) and, unusually, sphingosine[8]. The mechanism(s) leading to this complex pattern of storage remains unknown. How lipid storage causes neurodegeneration is also not understood. Current therapeutic approaches for NPC disease are limited[9]. No clinical benefit has been achieved by reducing cholesterol storage[10–12]. However, some benefit has been reported in a clinical trial using an inhibitor of GSL biosynthesis, miglustat[13,14]. These findings suggest that the mechanisms of pathogenesis are complicated and cannot be attributed to cholesterol or GSL storage alone.

An emerging factor in the pathogenesis of the primary lysosomal sphingolipid storage disorders (Gaucher disease, Sandhoff disease and GM1 gangliosidosis) is abnormal endoplasmic reticulum (ER) calcium homeostasis[15,16]. Owing to the similarity in stored sphingolipids (glucosylceramide (GlcCer), and GM1 and GM2 gangliosides) between NPC disease and the primary sphingolipidoses, we hypothesized that NPC1-mutant cells may also have altered calcium homeostasis.

In this study, we have found that, in contrast to the primary sphingolipidoses, NPC1-mutant cells have normal ER and mitochondrial calcium but substantially lower calcium in the acidic compartment. Chelation of calcium within the acidic compartment in healthy cells induces an NPC cellular disease phenotype. Pharmacological agents that elevate cytosolic calcium correct the NPC1 mutant cellular disease phenotypes *in vitro,* by compensating for reduced calcium release from the acidic compartment. These agents also improve function and life expectancy in a mouse model of NPC1 disease (here called the NPC1 mouse).

RESULTS

Defective lysosomal calcium homeostasis in NPC1-mutant cells

To determine whether calcium homeostasis is perturbed in NPC1 disease, we measured calcium release from the ER, mitochondria and the acidic compartment. Human B lymphoblasts were loaded with the calcium probe Fura-2AM and treated with either 100 μM ryanodine (**Fig. 1a**) or 1 μM thapsigargin (**Fig. 1a**) to release ER calcium or 2 μM carbonyl cyanide 3-chlorophenylhydrazone (CCCP), a mitochondrial uncoupler (**Fig. 1a**). No differences in calcium release from the ER or mitochondria were observed between normal and NPC1-mutant cells (**Fig. 1a**). However, when calcium was released from the acidic compartment with 200 μM Gly-Phe β-naphthylamide (GPN, whose hydrolysis by cathepsin C results in osmotic lysis of the acidic compartment, with a comparable rate of lysis in wild-type (WT) and NPC1-mutant cells, **Supplementary Fig. 1** online and **Fig. 1a**) or 500 nM bafilomycin A1 (an inhibitor of the vacuolar-ATPase; **Fig. 1a**),

[1]Department of Pharmacology, University of Oxford, Mansfield Road, Oxford OX1 3QT, UK. [2]Department of Genetics and Genomic Sciences, Mount Sinai School of Medicine, 1425 Madison Avenue, New York, New York 10029, USA. [3]Present address: Leicester School of Pharmacy, De Montfort University, The Gateway, Leicester LE1 9BH, UK. Correspondence should be addressed to E.L.-E. (emyr.lloyd-evans@pharm.ox.ac.uk) or F.M.P. (frances.platt@pharm.ox.ac.uk).

Received 1 April; accepted 5 September; published online 26 October 2008; doi:10.1038/nm.1876

we observed a ~65% reduction in NPC1-mutant cell calcium release from the acidic compartment compared to normal cells.

This reduction was confirmed in human NPC1-mutant fibroblasts, where calcium release from the acidic compartment induced by bafilomycin A1 was also reduced by ~70% compared to controls (**Fig. 1b**). To rule out ER involvement during measurement of acidic compartment calcium, we preincubated NPC1-mutant cells with thapsigargin followed by either GPN (**Fig. 1c**) or ionomycin followed by GPN (**Fig. 1d**) to induce calcium release from the acidic compartment alone. In all cases, we observed a reduction of ~70% in NPC1-mutant cell acidic compartment calcium compared to control cells, whereas ER (thapsigargin) or non-acidic compartment (ionomycin) calcium levels were identical.

We measured pH and calcium directly in the acidic compartment lumen with dextran-conjugated fluorescent reporters[17,18]. We determined acidic compartment pH in control and NPC1-mutant cells (**Fig. 1e**) in order to adjust the K_d (**Supplementary Fig. 2** online) of the low-affinity Rhod-dextran calcium probe (which records calcium without significant buffering)[17]. In agreement with a previous report[18], no difference was observed in the pH of the acidic compartment in NPC1-mutant cells relative to controls ($P = 0.112$). As the pH is equivalent in NPC1-mutant and control cells (**Fig. 1e**), we directly compared Rhod-dextran fluorescence (**Fig. 1f**). The fluorescence intensity of Rhod-dextran in the NPC1-mutant cell acidic compartment was reduced compared to controls (red/green (R/G) ratio reduced by 62%), and the calcium concentration was lowered from 550 μM to 209 μM. With these same methods (**Fig. 1e,f**) we determined the pH of the acidic compartment and the intralumenal calcium content of RAW macrophages treated with U18666A (a drug used to pharmacologically induce an NPC disease cellular phenotype). In agreement with the human subject–derived fibroblasts (**Fig. 1e**), we did not detect any difference in acidic compartment pH after 24 h of treatment with U18666A (untreated RAW cell pH, 4.01 ± 0.12; U18666A-treated RAW cell pH, 4.12 ± 0.13). Direct quantitative comparison of U18666A-treated macrophage acidic compartment calcium with Rhod-dextran also indicated a ~55–60% reduction in intralumenal acidic compartment calcium (**Fig. 1f**).

To determine whether reduced acidic compartment calcium has a role in NPC1 disease pathogenesis, we treated control cells with a high-affinity (strong calcium buffering) Rhod-dextran to chelate

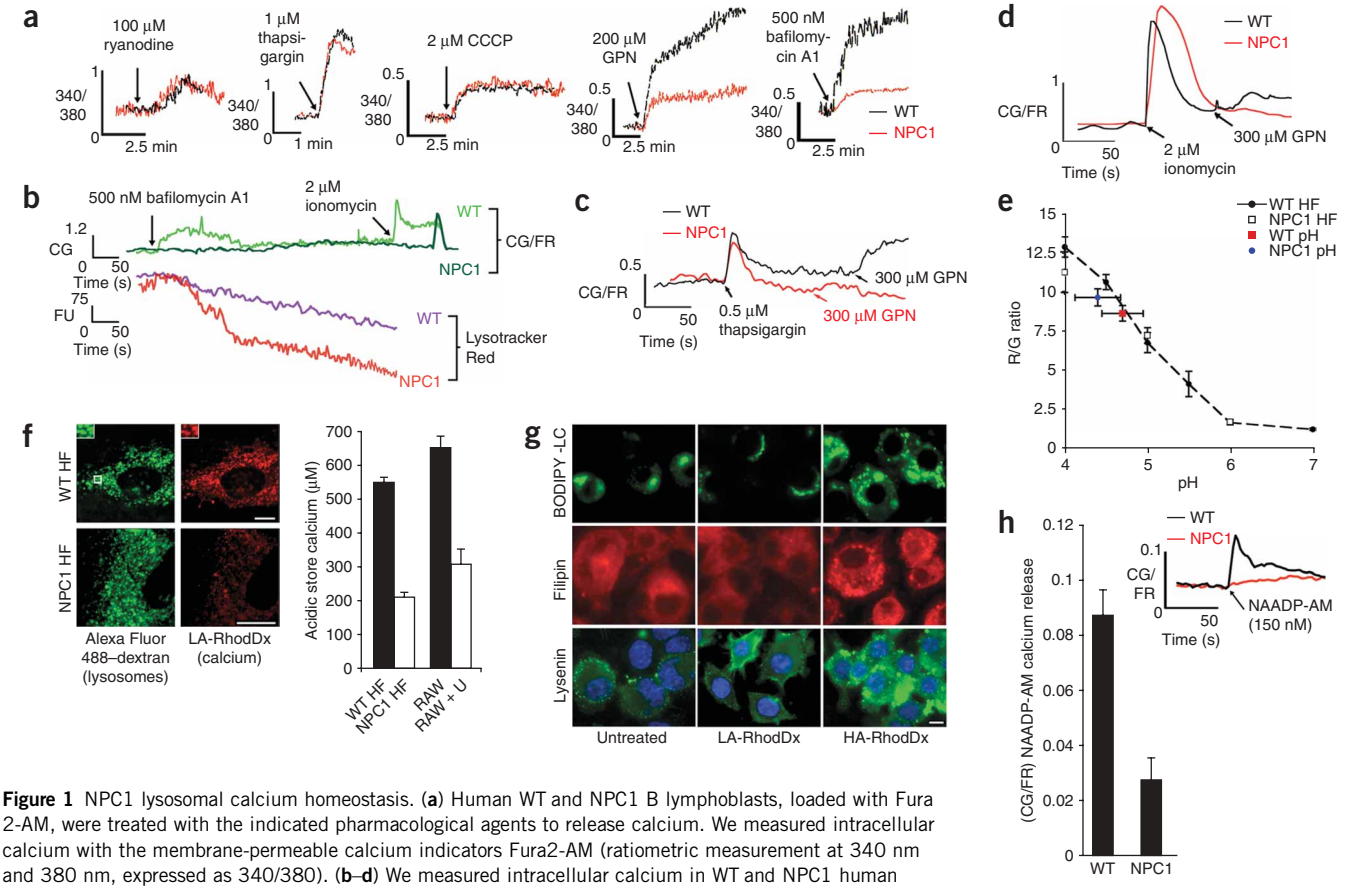

Figure 1 NPC1 lysosomal calcium homeostasis. (**a**) Human WT and NPC1 B lymphoblasts, loaded with Fura 2-AM, were treated with the indicated pharmacological agents to release calcium. We measured intracellular calcium with the membrane-permeable calcium indicators Fura2-AM (ratiometric measurement at 340 nm and 380 nm, expressed as 340/380). (**b–d**) We measured intracellular calcium in WT and NPC1 human fibroblasts (HF) with the membrane-permeable calcium indicator Calcium Green 1-AM and either Lysotracker Red (a fluorescent marker of the acidic compartment, **b**) or Fura Red–AM (expressed as the ratio of Calcium Green over Fura Red–AM, CG/FR, **c,d**). FU, arbitrary fluorescence units. (**e**) Standard curve to calculate endogenous lysosomal pH in HF ($P = 0.112$), R/G, red over green fluorescence ratio. (**f**) Left, fluorescence imaging of intralumenal compartment calcium in WT and NPC1 HF. Green, pH-insensitive dextran; Red, calcium-binding Rhod-dextran. Right, concentration of intralumenal acidic compartment calcium in WT and NPC1 HF, and in control or U18666A-treated RAW macrophages. U indicates U18666A treatment. LA–RhodDx, low-affinity Rhod-dextran. (**g**) Fluorescence images showing chelation of intralumenal acidic compartment calcium in RAW macrophages. Filipin stains cholesterol; lysenin stains sphingomyelin. BODIPY-LC, BODIPY-LacCer. HA–RhodDx, high-affinity Rhod-dextran. (**h**) We loaded HF with calcium probes (as in **c**) before addition of 0.5 μM thapsigargin followed by 150 nM NAADP-AM (inset is a representative calcium trace). The bar graph shows calcium release induced by NAADP-AM. Scale bars, 5 μm. $n = 3–6$ for each experiment (minimum of 50 cells analyzed per calcium trace). Error bars represent the means ± s.d.

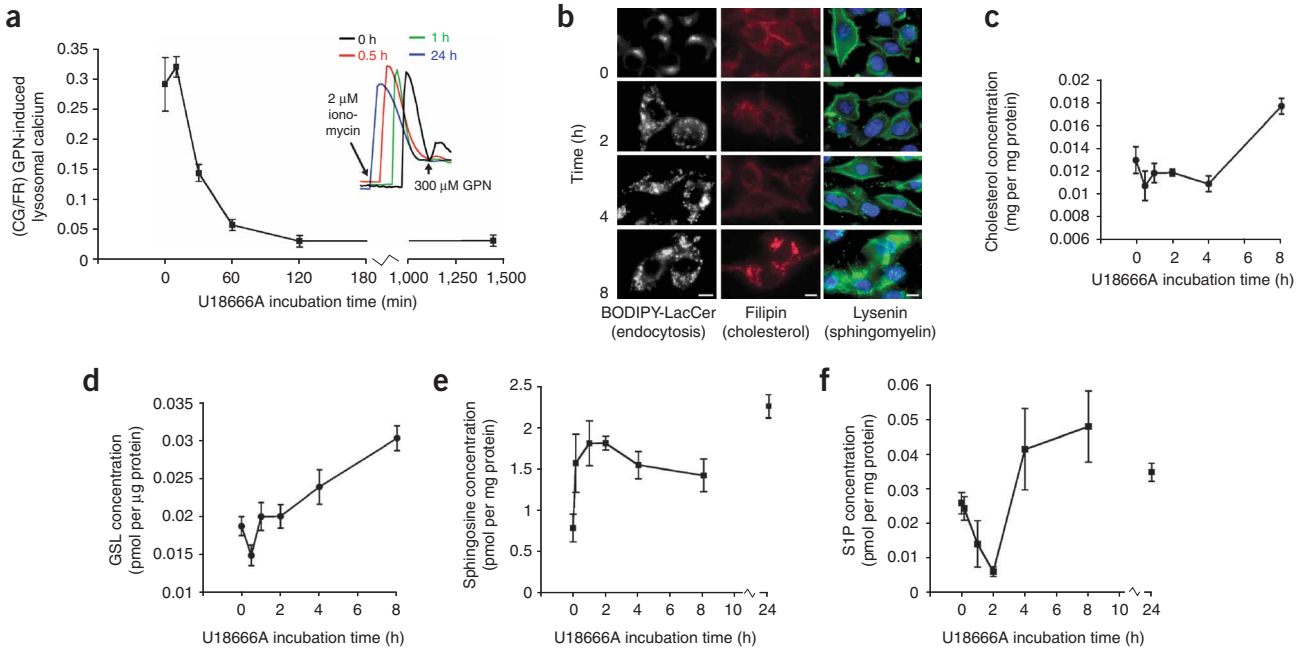

Figure 2 Abnormal lysosomal calcium is an early event during U18666A-induced NPC1 disease cellular phenotype. (**a**) We loaded RAW macrophages with Calcium Green 1–AM and Fura Red–AM after incubation with U18666A for the indicated times before acidic store calcium release (inset is a representative calcium trace). The main graph shows acidic compartment calcium content after GPN treatment over the indicated times. (**b**) Fluorescence images showing phenotypic changes in RAW cells after treatment with U18666A for the times indicated. Cells were labeled with either BODIPY-LacCer, filipin or lysenin and DAPI. Scale bar, 5 μm. (**c**–**f**) RAW cells treated with U18666A for the indicated times were harvested and analyzed to determine cholesterol (**c**), glycosphingolipids (GSL; **d**), sphingosine (**e**) and sphingosine-1-phosphate (S1P, **f**) concentrations. $n = 3$ or 4. Error bars represent the mean ± s.d.

intralumenal calcium. Pulse-chase treatment with calcium chelators into the acidic compartment for 7 h resulted in boron-dipyrromethene lactosylceramide (BODIPY-LacCer) mistrafficking and storage of cholesterol and sphingomyelin (**Fig. 1g**), all cellular hallmarks of NPC disease.

We next determined the signaling consequences of the calcium homeostatic defect. NAADP-AM is a cell membrane–permeant derivative of nicotinic acid adenine dinucleotide phosphate (NAADP)[19], the most potent calcium signaling second messenger[20]. It has recently been shown that NAADP releases calcium from the acidic compartment[21]. We pretreated control and NPC1-mutant human fibroblasts first with thapsigargin to rule out ER involvement during measurement of acidic compartment calcium, followed by 150 nM NAADP-AM (**Fig. 1h**) and observed a ~69% reduction in NPC1-mutant cell NAADP-induced calcium release (**Fig. 1h**), indicating functional reduction in the acidic compartment calcium store.

Calcium defect precedes cholesterol and GSL storage

We determined the kinetics of the reduction in calcium in the acidic compartment by inducing the NPC disease cellular phenotype in RAW macrophages with U18666A (**Fig. 2a**). Within 30 min after U18666A treatment, there was a reduction (~50%) in acidic compartment calcium released by GPN. A plateau was reached by 60–120 min after treatment (~80% reduction) that was sustained for 24 h.

The earliest measurable event after altered calcium homeostasis (**Fig. 2**) was altered sphingolipid trafficking (at 2 h; **Fig. 2b**), followed by acidic compartment storage of cholesterol (**Fig. 2b**), sphingomyelin (**Fig. 2b**) and GSLs (**Fig. 2d**), all at 8 h. These data were confirmed by biochemical analyses of cholesterol and GSLs (**Fig. 2c,d**).

Sphingosine is also stored in NPC1 disease. Therefore, sphingosine and its derivative sphingosine-1-phosphate (S1P) were measured by HPLC. Sphingosine was elevated at the earliest time point measured (10 min, **Fig. 2e**), remaining elevated for 24 h. There was a transient reduction in SIP levels during the first 2 h that recovered by 4 h (**Fig. 2f**). We measured acidic compartment calcium, endocytosis and cholesterol storage after washing out U18666A and found that acidic compartment calcium was the first defect to normalize, followed by correction in BODIPY-LacCer transport and finally by reduction in cholesterol levels (**Supplementary Fig. 3** online).

Sphingosine causes an acidic compartment calcium defect

To test whether one of the individual lipids known to be stored in NPC disease was capable of inducing the acidic compartment calcium defect, we exogenously added each lipid to RAW cells before release of lysosomal calcium. Only sphingosine was capable of inducing the abnormal calcium phenotype (**Fig. 3a**). This effect was concentration dependent, as it was induced by 1 μM but not 0.1 μM sphingosine (**Fig. 3b**), concentrations that do not have detergent effects (1–2 μM), unlike 10 μM sphingosine (**Fig. 3c**). The calcium defect was not observed with 1 μM sphinganine (**Fig. 3b**).

RAW cells treated with 2 μM sphingosine for 24 h showed elevated Lysotracker (**Fig. 3c**) and cholesterol (filipin, **Fig. 3d**) staining, which are recognized NPC disease cellular phenotypes[13]. Elevated cholesterol staining was observed with 1 μM but not 0.1 μM sphingosine (**Fig. 3d**), correlating with the concentration-dependent effect on calcium homeostasis (**Fig. 3b**). We analyzed the effect of exogenous sphingosine (2 μM) on RAW macrophages over 24 h (**Fig. 3e**). Reduced acidic compartment calcium induced by sphingosine was evident 10 min after treatment, reaching maximal reduction by

30 min, and was sustained until 24 h after treatment (**Fig. 3e**). We also observed altered endocytic trafficking at 2 h (BODIPY-LacCer), and cholesterol storage (filipin) at 8 h after sphingosine treatment (**Fig. 3f**). This is the same order of events that we observed after alteration in acidic compartment calcium by U18666A treatment (**Fig. 2b**). Reduction of sphingosine levels (**Fig. 3**) with ISP1 (inhibitor of serine palmitoyl transferase 1, also known as myriocin) corrected all NPC1-mutant cellular phenotypes, with lysosomal calcium returning to control levels first (**Fig. 3h**), followed by trafficking correction, then reduced lipid storage (**Fig. 3g**). Sphingosine treatment did not further alter the calcium levels of NPC1-mutant fibroblasts (data not shown). Tetramethyl-rhodamine (TMR)–sphingosine induced an NPC disease cellular phenotype and was found associated with lysosomes within 10 min (**Supplementary Fig. 4** online).

Correction of NPC1 cells with calcium-modulating drugs

Endocytic fusion and transport events are dependent on calcium release from the acidic compartment[22]. Defective calcium release is predicted to result in defective endocytic transport, fusion or both[22], potentially leading to NPC disease cellular phenotypes (**Fig. 1g**,**h**). Prolonged elevation in cytosolic calcium, caused by mobilizing calcium from, for example, the ER, has the potential to overcome NPC1 disease acidic compartment transport defects. Thapsigargin increases cytosolic calcium by releasing ER calcium via inhibition of the sarco(endo)plasmic reticulum ATPase (SERCA). NPC1-mutant CHO cells (confirmed as having reduced acidic compartment calcium using the calcium probes Calcium Green–1AM and Fura Red–AM (values are arbitrary fluorescent units), CHO WT, 0.107 ± 0.047; CHO NPC1-null, 0.018 ± 0.003) had reduced acidic compartment fusion (**Fig. 4a**). Thapsigargin-induced elevation in cytosolic calcium did not increase NPC1-mutant CHO cell acidic compartment calcium but did elevate WT CHO cell acidic compartment calcium (**Supplementary Figs. 5** and **6** online). Treatment of NPC1-mutant cells with thapsigargin for 30–60 min induced fusion between late endosomes and lysosomes (**Fig. 4a**). Horseradish peroxidase (HRP) uptake in NPC1-mutant cells is defective due to Annexin A2 mislocalization. Treatment of NPC1-mutant CHO cells with 1 μM thapsigargin for 1 h led to relocalization of Annexin A2 back to peripheral endosomes (**Fig. 4b**), which is responsible for correction in endocytic uptake of HRP (**Fig. 4b**) and associated with correction of defective

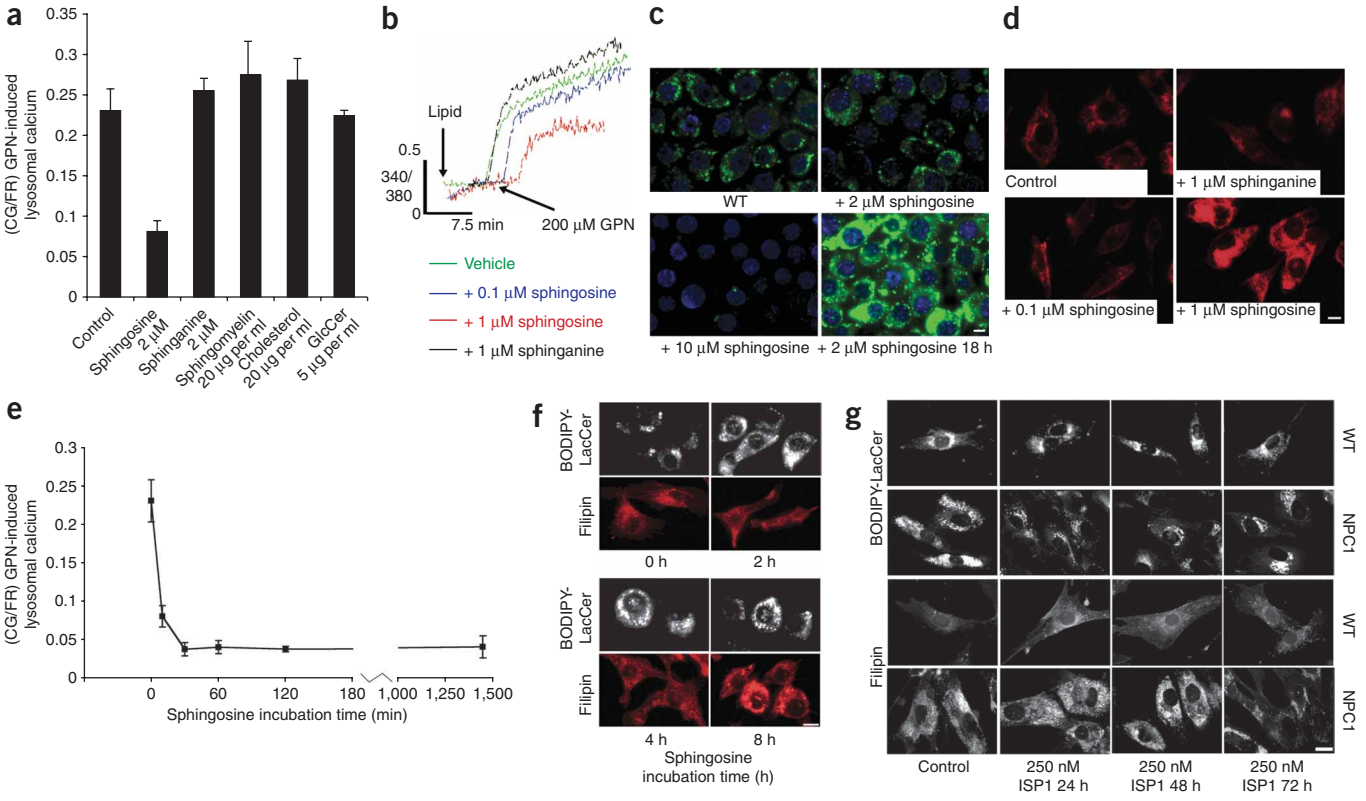

Figure 3 Sphingosine specifically reduces lysosomal calcium. (**a**) RAW macrophage lysosomal calcium content, as estimated after addition of 2 μM ionomycin and 300 μM GPN. (**b**) WT B lymphoblasts were pretreated with the indicated concentration of lipid for 10 min before release of lysosomal calcium. We measured intracellular calcium with the membrane-permeable calcium indicator Fura2-AM (ratiometric measurement at 340 nm and 380 nm, expressed as 340/380). (**c**) Fluorescence imaging of RAW macrophages incubated with different concentrations of sphingosine (for 10 min where not indicated or for 18 h) and loaded with Lysotracker Green (a fluorescent marker of the acidic compartment). (**d**) Filipin staining showing the effect of sphingoid bases on RAW macrophage cholesterol. (**e**) RAW macrophages were incubated with 2 μM sphingosine for the indicated times before addition of 2 μM ionomycin and followed by addition of 300 μM GPN. Then, we measured lysosomal calcium. (**f**) Imaging of RAW macrophages after treatment with 1 μM sphingosine for the indicated times; cells were labeled with either BODIPY-LacCer or filipin. (**g**) Imaging of WT and NPC1 HF for the indicated times with ISP1 and stained with BODIPY-LacCer or filipin. (**h**) Acidic store calcium release in HFs treated as indicated and loaded with Calcium Green 1–AM and Fura Red–AM. Scale bar, 5 μm. $n = 3$–5. Error bars represent the mean ± s.d.

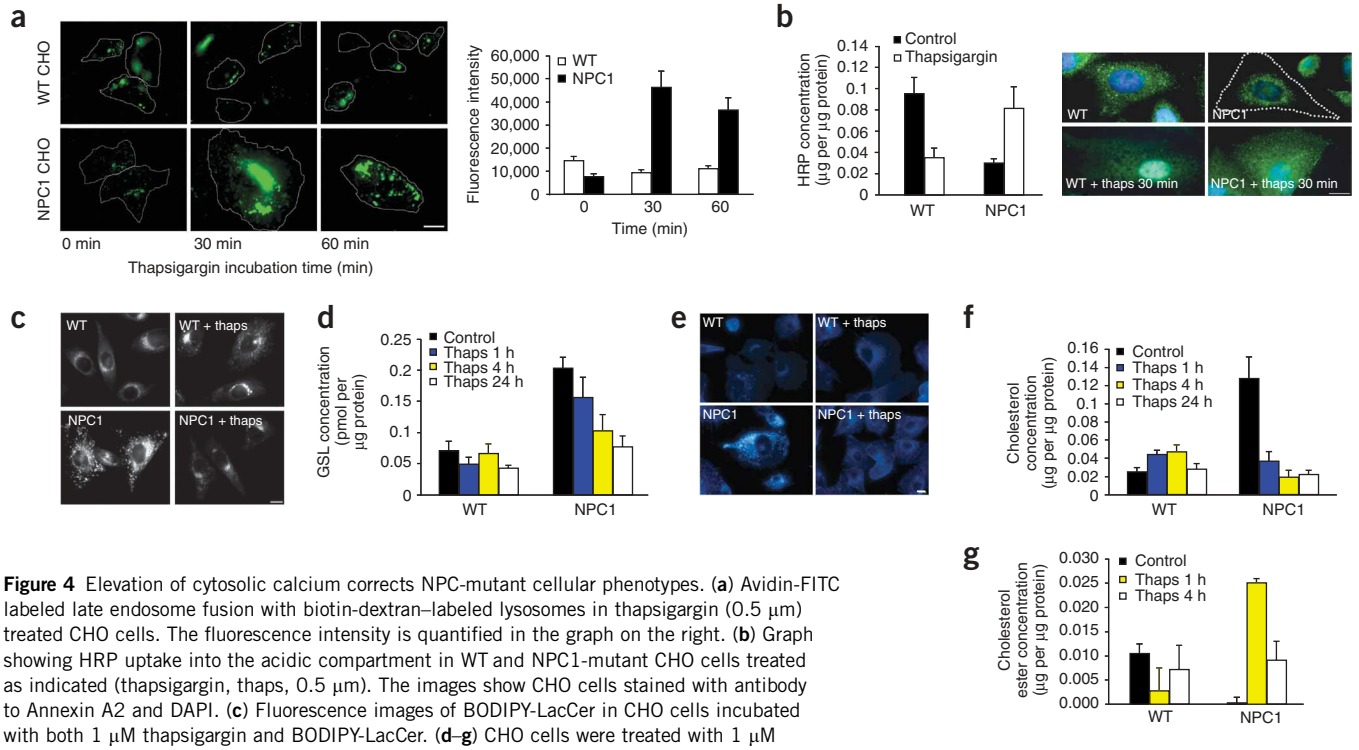

Figure 4 Elevation of cytosolic calcium corrects NPC-mutant cellular phenotypes. (**a**) Avidin-FITC labeled late endosome fusion with biotin-dextran–labeled lysosomes in thapsigargin (0.5 μm) treated CHO cells. The fluorescence intensity is quantified in the graph on the right. (**b**) Graph showing HRP uptake into the acidic compartment in WT and NPC1-mutant CHO cells treated as indicated (thapsigargin, thaps, 0.5 μm). The images show CHO cells stained with antibody to Annexin A2 and DAPI. (**c**) Fluorescence images of BODIPY-LacCer in CHO cells incubated with both 1 μM thapsigargin and BODIPY-LacCer. (**d**–**g**) CHO cells were treated with 1 μM thapsigargin as indicated. (**d**) Analysis of glycosphingolipid concentration, (**e**) visualization of cholesterol with filipin, (**f**) analysis of cholesterol concentration and (**g**) analysis of cholesterol ester concentration. Scale bar, 5 μm. $n = 3$; error bars represent the means ± s.d.

BODIPY-LacCer transport (**Fig. 4c**). Treatment of WT cells with 1 μM thapsigargin was associated with relocalization of Annexin A2 to reticular (possibly ER) structures, potentially explaining the reduced HRP uptake in WT cells (**Fig. 4b**). This was associated with a time-dependent reduction in GSLs to WT levels after 24 h (**Fig. 4d**). Cholesterol localization (filipin, **Fig. 4e**) and levels (**Fig. 4f**) were near normal after 24 h of thapsigargin treatment. Cholesterol ester levels were near normal by 4 h after thapsigargin treatment, consistent with cholesterol transport to the ER (**Fig. 4g**).

Efficacy of curcumin therapy in the NPC1 mouse

As thapsigargin is relatively toxic *in vivo*, we evaluated the weaker SERCA antagonist curcumin, a natural product derived from turmeric[23]. Cultured NPC1-mutant mouse glial cells grown in the presence of 30 μM curcumin for 1 h had normalized sphingolipid trafficking (**Fig. 5a**) analogous to that achieved with thapsigargin (**Fig. 4c**). Co-incubation of NPC1-mutant glial cells with curcumin and the intracellular calcium chelator BAPTA-AM prevented the normalization in sphingolipid trafficking (**Fig. 5a**) and cholesterol levels (data not shown), indicating that the beneficial effect is due to increased cytosolic calcium rather than sequestration of calcium (**Supplementary Fig. 6**) into the acidic compartment or antioxidant effects.

We tested the therapeutic effects of oral curcumin (150 mg kg^{-1} d^{-1} from weaning) in the NPC1 mouse. Curcumin-treated NPC1 mice had improved coat condition (**Fig. 5b**), improved weight gain (**Fig. 5c**), increased activity (**Fig. 5d**) and reduced tremor (**Fig. 5e**) compared to untreated NPC1 mice. Curcumin-fed NPC1 mice also survived 3.5 weeks longer than untreated mice (~35% improvement, $P < 0.0001$; **Fig. 5f**). The curcumin-treated NPC1 mice had lower levels of total brain GSL storage at 9 weeks of age (**Fig. 5g**,**h**). Sphingosine levels were elevated ~2.5 fold in NPC1 mouse brain at 9 weeks of age (**Fig. 5i**) and were not significantly changed after curcumin treatment. S1P levels increased six- to sevenfold in NPC1 versus wild-type mouse brain and were reduced almost to WT levels after curcumin therapy (**Fig. 5j**).

DISCUSSION

NPC disease is a complex lipid storage disorder that results from inactivation of the NPC1 or NPC2 protein[1]. This results in a poorly understood series of events that ultimately leads to neurodegeneration and premature death. Recently, several publications have raised the possibility that cholesterol may not be the primary toxic metabolite in NPC1 disease[4,24–26]. Defining the early step(s) in the pathogenic cascade has the potential to increase our understanding of NPC1 function and to lead to the identification of novel clinical intervention points.

The relative pathological importance of the various lipids that accumulate in NPC disease remains controversial. In this study, we have determined the chronology of events after inactivation of NPC1. The first detectable change was an increase in acidic compartment sphingosine levels and a concomitant decrease in SIP. Sphingosine elevation occurred very rapidly, within 0–60 min after drug treatment, and then plateaued, suggesting compensatory changes within the cell. Notably, the decrease in S1P was transient, as S1P levels increased back to control levels 4 h after treatment. This suggests that the lysosome is the main source of sphingosine for S1P production in healthy cells, but that the cell can compensate for a loss of availability of this pool of sphingosine, possibly by upregulating the activity of other ceramidases[27].

Sphingosine generated from ceramide degradation in the lysosome is protonated (pK_a of 8.9 (ref. 28)) and does not cross the lysosomal membrane unless facilitated by a transporter. On the basis of our data, NPC1 emerges as a candidate for involvement in sphingosine efflux

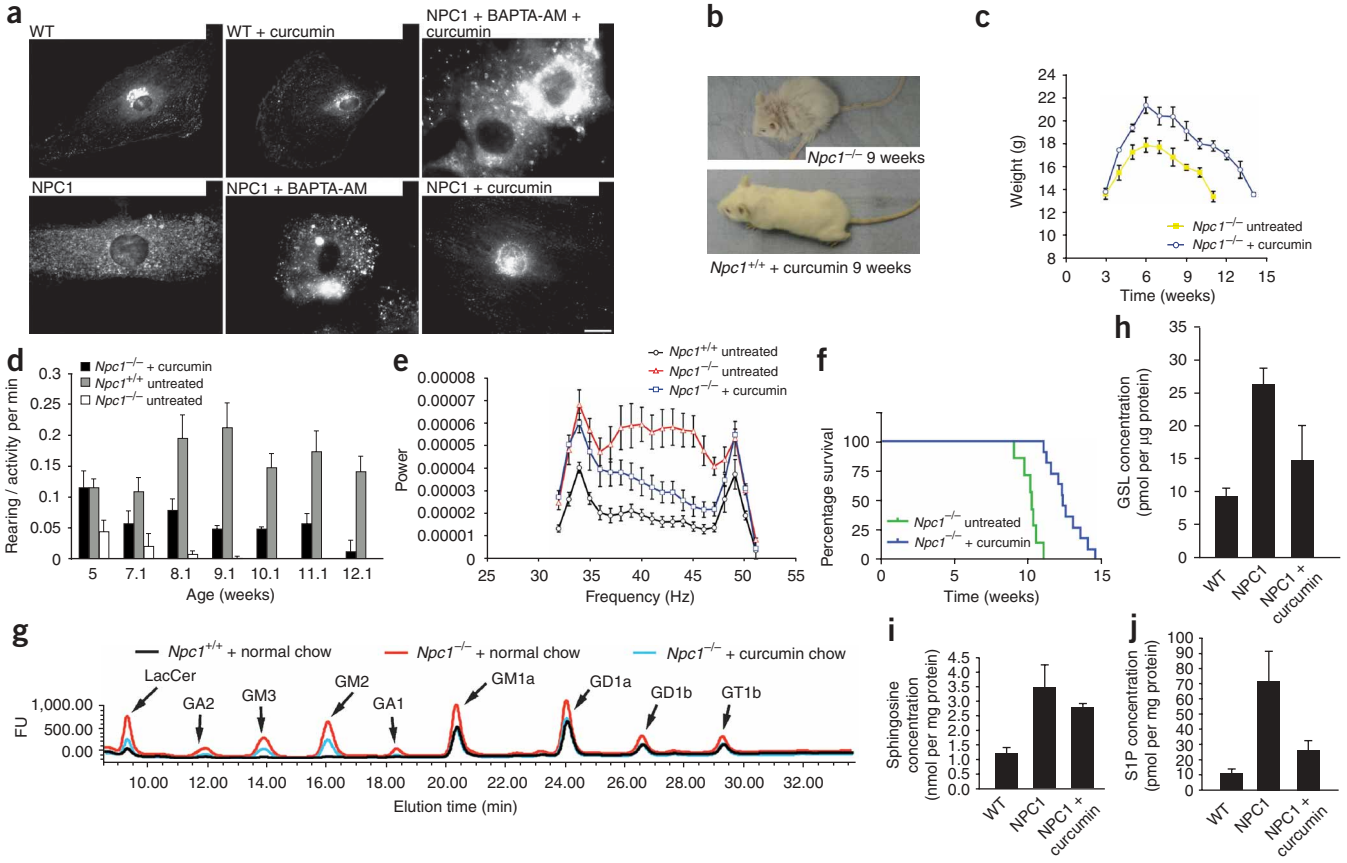

Figure 5 Increased survival and improved function in NPC1 mice treated with curcumin. (**a**) Fluorescence imaging of BODIPY-LacCer in WT and NPC1 mouse astroglia incubated with 30 µM curcumin, 50 µM BAPTA-AM or both and BODIPY-LacCer. (**b**) Nine-week-old untreated and curcumin-treated NPC1 mice. (**c**) Weights of untreated and curcumin-treated NPC1 mice. (**d**) Open-field analysis for WT (*Npc1* $^{+/+}$), untreated NPC1 (*Npc1*$^{-/-}$) and curcumin-treated *Npc1*$^{-/-}$ mice. (**e**) Tremor analysis of WT (*Npc1*$^{+/+}$, black), untreated NPC1 (*Npc1*$^{-/-}$, red) and curcumin-treated *Npc1*$^{-/-}$ (blue) mice at 9 weeks of age. (**f**) Survival of untreated and curcumin-treated NPC1 mice. (**g**) HPLC profiles of glycosphingolipids extracted from whole brains of 9-week-old WT, untreated NPC1-null and curcumin-treated NPC1 mice with the major GSL species indicated (minor unknown GSL peaks not annotated). (**h**) Quantification of traces, including data from all peaks, as total glycosphingolipids. Sphingosine (**i**) and S1P levels (**j**) in 9-week-old WT, untreated NPC1 and curcumin-treated NPC1 mice ($P = 0.149$ for sphingosine values of untreated NPC1 and curcumin-treated NPC1 mice). Scale bar, 5 µm. $n = 5$ separate repeats per experiment with five to eight mice per repeat. Each graph (except survival, where each point is an individual death) represents the mean ± s.d.

from lysosomes. When NPC1 protein is inactivated, sphingosine rapidly accumulates in the lysosome, and there is reduced efflux of sphingosine from the lysosome, which is a key step in the salvage pathway of GSL biosynthesis and S1P generation[29,30]. Sphingosine-1-phosphate is an essential signaling lipid that regulates many processes[31], including the transcription of several cholesterol biosynthetic enzymes[32]; thus NPC1 may determine the fate of cholesterol passing through the endocytic system by facilitating the efflux of sphingosine to generate S1P, which, in turn, regulates aspects of cholesterol metabolism.

After sphingosine storage, the subsequent event in NPC disease pathogenesis is abnormally low acidic compartment calcium concentration. This is caused by sphingosine storage, as sphingosine, when exogenously added to healthy cells, is the only lipid that is stored in NPC disease that induces this phenotype. This sphingosine storage effect on calcium was rapid, suggesting a direct effect of sphingosine rather than of a downstream metabolite. We have calculated that these sphingosine storage levels (~0.75 µM in U18666A-treated RAW cells and ~1.5 µM in NPC1 mouse brain) approximate the exogenous sphingosine concentrations (~1 µM) required to decrease acidic compartment calcium and induce an NPC disease cellular phenotype. It is likely that sphingosine storage inhibits calcium uptake into the acidic compartment (**Supplementary Fig. 5**), so there is insufficient calcium release for fusion, trafficking or both in the endocytic pathway. Sphingosine is a known inhibitor of protein kinase C, calcium ATPases and Na^+/Ca^{2+} exchangers, and it may inhibit calcium entry into the acidic compartment by similar mechanisms[33]; the inhibitory effect of sphingosine on protein kinase C has recently been identified as a possible cause of the Rab 9 (small GTPase)-associated endocytic dysfunction in NPC1 disease[34]. The defect in acidic compartment calcium homeostasis does not require protons, as the acidic compartment in NPC1-mutant cells maintains normal pH, in agreement with a previous report[18].

In this study, we observed normal ER and mitochondrial calcium homeostasis in NPC disease cells. These data suggest that, in contrast to the primary glycosphingolipidoses, stored GSLs in NPC disease cells cannot reach the ER and are instead trapped in the acidic compartment, further illustrating that a transport defect occurs before lipid storage. Our findings of normal ER calcium homeostasis in NPC1-mutant cells are in agreement with a previous report in which depolarization leading to ER calcium release was identical between control and NPC1-mutant primary neurons[35,36].

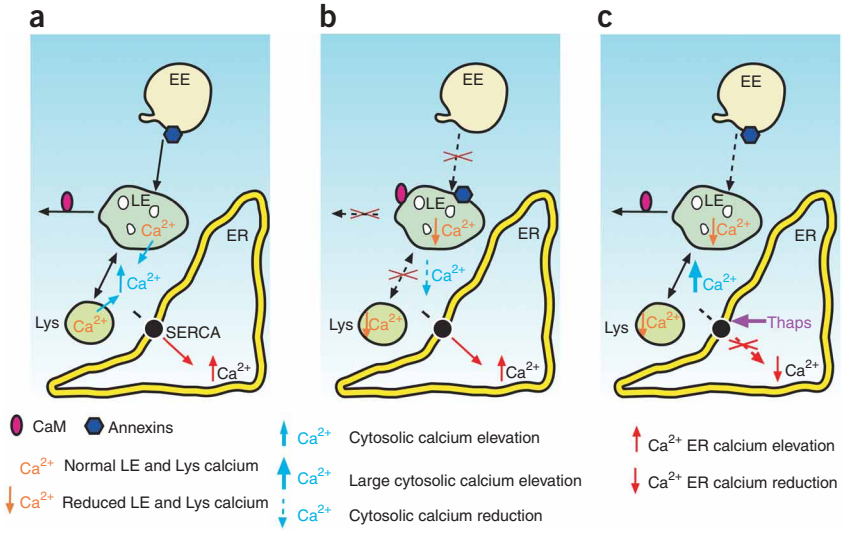

Figure 6 Curcumin-induced elevation in cytosolic calcium overcomes reduced lysosomal calcium and corrects endocytic transport in NPC1-null cells. (**a**) Numerous endocytic transport steps are dependent on the function of calcium-dependent protein machinery, such as annexins and calmodulin. (**b**) Depletion of lysosomal calcium caused by sphingosine storage in NPC1 disease leads to impaired endocytic function and subsequent lipid storage. (**c**) Prolonged elevation of cytosolic calcium overcomes defective lysosomal calcium release, allowing endocytosis to continue via calcium-dependent proteins, such as Annexin A2 (**Fig. 4b**). EE, early endosome; CaM, calmodulin; LE, late endosome; Lys, lysosome.

Calcium entry and egress from acidic stores is regulated by specific activities. Late endosome and lysosome calcium store filling occurs via a heavy metal–inhibitable and ATP-dependent process, presumably through a channel[37]. Calcium entry does not occur through passive internalization of extracellular calcium by endocytosis[17]. Calcium release via the NAADP receptor[20] from the acidic compartment has been shown to be crucial for endocytic transport and fusion events[22]. Consistent with these data, the reduction in acidic store calcium filling (**Supplementary Fig. 5** and **Fig. 6**) and the subsequent reduced NAADP-mediated calcium release in NPC1 disease has profound effects on endocytic transport and fusion.

We tested the possibility that depletion of acidic compartment calcium leads to a perturbation of endocytosis and subsequent NPC disease lipid storage by specifically chelating calcium in the acidic compartment. The calcium concentration of the acidic compartment has been estimated to be approximately 200–600 μM[17,38]. High-affinity Rhod-dextran at acidic pH has an estimated K_d for calcium of ~5 μM, enough to chelate the compartment. Treatment with high-affinity Rhod-dextran led to very rapid (within 4 h) generation of an NPC disease cellular phenotype. Our findings illustrate that perturbation of acidic compartment calcium can lead to defective endocytosis and subsequent storage of lipids in the acidic compartment, similar to that seen in NPC disease. This perturbation in endocytosis is potentially caused by a combination of defective vesicular fusion and trafficking events that are mediated by calcium release from the acidic compartment and by calcium-dependent accessory proteins. Calmodulin inhibitors, such as W-7 and calmidazolium, are capable of inducing an NPC disease cellular phenotype[39]. Perturbation in the function of Annexin A2 (a calcium- and phospholipid-binding protein) has been shown to cause defective early to late endosome transport in NPC1-mutant cells[40]. The decreased acidic compartment calcium in NPC disease may account for this perturbation, as changes in intracellular calcium can alter Annexin function and localization[41]. Thus, a key finding of this study is that cholesterol, sphingomyelin and GSL storage are downstream events in NPC disease pathogenesis caused by sphingosine storage, leading to altered acidic compartment calcium levels, which, in turn, inhibit the endocytic pathway.

Our findings are in agreement with recent studies showing that the sterol binding capacity of the NPC1 protein is non-essential for rescuing NPC1 deficient cells, suggesting a cholesterol-independent mechanism of inducing NPC1 disease. Our study suggests that sphingosine is the key NPC1 storage lipid for inducing pathogenesis and implicates NPC1 in facilitating sphingosine efflux from lysosomes.

We evaluated two agents (thapsigargin and curcumin), neither of which correct the calcium content of the acidic compartment (**Supplementary Fig. 5**) but that compensate for lack of calcium release from the acidic compartment by elevating calcium levels in the cytosol (**Fig. 1a,c** and **Fig. 6**). These drugs normalize the fusion and trafficking machinery in NPC1-mutant cells by increasing the calcium levels in the cytosol that can be used by the calcium-dependent proteins, such as Annexin A2, that are necessary for the normal function of the endocytic pathway. Both drugs corrected the NPC1 disease phenotype at the cellular level. We tested curcumin (a weak SERCA antagonist with low toxicity) in the NPC1 mouse. It resulted in increased life expectancy (35%) and slowed the rate of disease progression (by 3 weeks). These data suggest a potential new therapeutic strategy for NPC1 disease treatment—using agents that can compensate for the underlying calcium homeostatic defect. Elevated lipid levels in NPC1 mouse brain were reduced after curcumin treatment, including that of S1P, which may be a result of reduced macrophage infiltration[42]. Sphingosine levels were unchanged, consistent with sphingosine storage being the primary defect (**Figs. 5i** and **6**).

In summary, we have identified sphingosine storage as the earliest measurable event after induction of an NPC disease phenotype. This induces a novel calcium homeostatic defect characterized by low calcium levels in acidic stores. This finding may explain why there is such a profound block in late endosome to lysosome transport in NPC disease, resulting in downstream storage of cholesterol and GSLs. These data therefore suggest a new mechanism of pathogenesis in NPC disease and identify a new clinical intervention strategy for treating this neurodegenerative disorder in the future.

METHODS

Mice. We maintained *Npc1*$^{-/-}$ and *Npc1*$^{+/+}$ mice (a gift from R. Lachmann) as previously described[8]. We mixed curcumin (Sigma) as a dry solid with powdered mouse (SDS) chow, pelleted it and fed it to mice to at a dose of 150 mg kg^{-1} d^{-1}. We conducted all mouse studies with protocols approved by the UK Home Office for the Conduct of Regulated Procedures under license (Animal Scientific Procedures Act, 1986). All protocols were approved by both the Departmental Ethical Review and University Animal Care and Ethical Review committees.

Cells. We obtained human NPC1-mutant and control fibroblasts (GM03123 and GM05399, respectively) and B lymphoblasts (GM03124 and GM03299, respectively) from the Coriell cell repository; these NPC-mutant cells have been

documented to have no NPC1 protein expression[43]. NPC1-mutant CHO cells (CT43) and controls (RA25) were a gift from T.Y. Chang. We isolated *Npc1*$^{-/-}$ and *Npc1*$^{+/+}$ mouse brain glia and maintained them in tissue culture as previously described[44] from newborn mouse pups (post-natal day 1); we confirmed their genotypes by PCR[8]. We grew all cells at 37 °C with 5% CO_2 in either RPMI (lymphoblasts), DMEM (fibroblasts and glia) or Ham's F-12/DMEM (CHO cells) with 10% FCS, 1% penicillin-streptomycin and 1% L-glutamine (Lonza). We treated cells with U18666A at a concentration of 2 μg/ml.

pH measurement. We measured lysosomal pH as previously described[18] with minor modifications. We loaded fluorescein-dextran and rhodamine-dextran (Sigma) at 0.25 mg ml^{-1} for 12 h into cells at 37 °C followed by a 12-h chase at 37 °C to label lysosomes. We generated the standard curve by treating cells with buffers adjusted to a series of defined pH values in conjunction with valinomycin and nigericin (which collapse the membrane potential to facilitate equilibration with external buffer). We performed image analysis and quantification of fluorescence with SimplePCI software (Hamamatsu).

Calcium assays. We carried out lysosomal calcium measurements as previously described[17] with minor modifications. For documenting calcium concentration, we used low-affinity Rhod-dextran (K_d = 551 ± 107 μM) in conjunction with the calcium-insensitive Alexa-Fluor 488–dextran (Invitrogen) at concentrations of 0.25 mg ml^{-1} and 0.1mg ml^{-1}, respectively. We loaded the cells for the same time and under the same conditions as for the pH measurements. We measured intracellular calcium with the membrane-permeable calcium indicators Fura2-AM alone or Calcium Green 1–AM in conjunction with Fura Red–AM (all at 5 μM, Molecular Probes). We loaded the cells as previously described[45] for 1 h at 20 °C before washing them and visualizing calcium release either on a Zeiss LSM 510 confocal microscope for adherent cells or by cuvette-based recording on a Jasco FP-777 (with calcium-recording module CA-261) for non-adherent cells. All agents were added in DMSO (final concentrations did not exceed 0.5% volume); NAADP-AM was added in HBSS buffer. We analyzed movies with Magipix and Magigraph software (developed and distributed by R. Jacob).

Sphingosine and sphingosine-1-phosphate measurement. We performed measurements as previously described[46].

Glycosphingolipid measurement. We performed measurements as previously described[47].

Cholesterol measurement. We quantified cholesterol and cholesterol esters with the Amplex Red Molecular Probes kit according to the manufacturer's instructions. We visualized cellular cholesterol with filipin (Polysciences) as previously described[8].

Sphingomyelin measurement. We visualized intracellular sphingomyelin with lysenin (Peptides International) as previously described[48] with minor modifications. We incubated paraformaldehyde-fixed (4%, 15 min) cells with lysenin (0.1 μg ml^{-1}) for 12 h at 4 °C before washing them and incubating them with primary antibody to lysenin at 20 °C for 1 h, followed by incubation with fluorescent secondary antibody (conjugated to Alexa Fluor 488, Molecular Probes) at 20 °C for 30 min. We washed the cells, mounted them on glass slides in Mowiol (Merck) and examined them with a Zeiss Axiovert fluorescence microscope. We captured images with a charge-coupled device camera and Axiovision 3.1 software.

BODIPY-lactosylceramide transport. We performed BODIPY-lactosylceramide transport as previously described[8] with minor modifications. We used BODIPY-LacCer (Molecular Probes) at a concentration of 7.5 μM with an initial incubation for 45 min at 20 °C followed by a 1-h chase at 37 °C and three 5-min washes in medium containing 10% FCS and 1% BSA.

Lysotracker staining of lysosomes. We live-stained cells with 200 nM Lysotracker Green (Molecular Probes) in PBS at 20 °C for 10 min before washing and visualizing them.

Horseradish peroxidase uptake. We performed HRP uptake as previously described[8].

Late endosome–lysosome fusion assay. We performed late endosome–lysosome fusion assays as previously described[49] with Oregon Green–avidin (Molecular Probes) as the indicator of endosome fusion (0.1 mg ml^{-1}, 10-min pulse and 20-min chase at 37 °C) and biotin-dextran (Molecular Probes) as the lysosomal marker (0.1 mg ml^{-1}, 12-h pulse and 12-h chase at 37 °C). After these incubations, we measured endosome-lysosome fusion as the increase in Oregon Green–avidin fluorescence upon binding to biotin-dextran. Each time point represents a new coverslip of cells incubated with 1-μM thapsigargin for the indicated time.

Open field analysis. We performed open-field analysis as described previously[50].

Tremor. We measured tremor in mice with a commercial tremor monitor (San Diego Instruments) according to the manufacturer's instructions. We monitored the mice for 256 s.

Statistical analyses. All statistical analyses were performed with Prism software (Microcal).

Note: Supplementary information is available on the Nature Medicine website.

ACKNOWLEDGMENTS

NPC1-mutant CHO cells (CT43) and controls (RA25) were a gift from T.Y. Chang (Dartmouth Medical School). *Npc1*$^{-/-}$ and *Npc1*$^{+/+}$ mice were a gift from R. Lachmann (University of Cambridge). Magipix and Magigraph software were developed and distributed by R. Jacob (Kings College London). E.L.-E. was supported by grants from the Ara Parseghian Medical Research Foundation and Birth Defects Foundation Newlife. A.J.M. was supported by the Wellcome Trust, UK. X.H. was supported by NIHR01 DK54830. D.A.S. was supported by the National Niemann-Pick Disease Foundation USA. E.E.-S. was supported by the Glycobiology Institute, Oxford University. D.J.S. was supported by the Ara Parseghian Medical Research Foundation. We thank D. Jelfs and J. Freeman for expert technical assistance. We are indebted to the UK Niemann-Pick Disease Group for their interest and support of this research.

AUTHOR CONTRIBUTIONS

E.L.-E., F.M.P., A.J.M. and A.G. devised and/or performed the experiments. E.H.S. and X.H. carried out sphingosine and S1P analysis, D.A.S. and E.E.-S. carried out behavioral analysis, D.J.S. and G.C.C. provided methods and reagents, and E.L.-E. and F.M.P. wrote the manuscript.

Published online at http://www.nature.com/naturemedicine/
Reprints and permissions information is available online at http://npg.nature.com/reprintsandpermissions/

1. Vanier, M.T. & Millat, G. Niemann-Pick disease type C. *Clin. Genet.* **64**, 269–281 (2003).
2. Ko, D.C., Gordon, M.D., Jin, J.Y. & Scott, M.P. Dynamic movements of organelles containing Niemann-Pick C1 protein: NPC1 involvement in late endocytic events. *Mol. Biol. Cell* **12**, 601–614 (2001).
3. Liscum, L. Niemann-Pick type C mutations cause lipid traffic jam. *Traffic* **1**, 218–225 (2000).
4. Davies, J.P., Chen, F.W. & Ioannou, Y.A. Transmembrane molecular pump activity of Niemann-Pick C1 protein. *Science* **290**, 2295–2298 (2000).
5. Naureckiene, S. *et al.* Identification of *HE1* as the second gene of Niemann-Pick C disease. *Science* **290**, 2298–2301 (2000).
6. Babalola, J.O. *et al.* Development of an assay for the intermembrane transfer of cholesterol by Niemann-Pick C2 protein. *Biol. Chem.* **388**, 617–626 (2007).
7. Butler, J.D., Vanier, M.T. & Pentchev, P.G. Niemann-Pick C disease: cystine and lipids accumulate in the murine model of this lysosomal cholesterol lipidosis. *Biochem. Biophys. Res. Commun.* **196**, 154–159 (1993).
8. te Vruchte, D. *et al.* Accumulation of glycosphingolipids in Niemann-Pick C disease disrupts endosomal transport. *J. Biol. Chem.* **279**, 26167–26175 (2004).
9. Patterson, M.C. & Platt, F. Therapy of Niemann-Pick disease, type C. *Biochim. Biophys. Acta* **1685**, 77–82 (2004).
10. Patterson, M.C. *et al.* The effect of cholesterol-lowering agents on hepatic and plasma cholesterol in Niemann-Pick disease type C. *Neurology* **43**, 61–64 (1993).
11. Erickson, R.P., Garver, W.S., Camargo, F., Hossain, G.S. & Heidenreich, R.A. Pharmacological and genetic modifications of somatic cholesterol do not substantially alter the course of CNS disease in Niemann-Pick C mice. *J. Inherit. Metab. Dis.* **23**, 54–62 (2000).

12. Somers, K.L. *et al.* Effects of dietary cholesterol restriction in a feline model of Niemann-Pick type C disease. *J. Inherit. Metab. Dis.* **24**, 427–436 (2001).
13. Lachmann, R.H. *et al.* Treatment with miglustat reverses the lipid-trafficking defect in Niemann-Pick disease type C. *Neurobiol. Dis.* **16**, 654–658 (2004).
14. Patterson, M.C., Vecchio, D., Prady, H., Abel, L. & Wraith, J.E. Miglustat for treatment of Niemann-Pick C disease: a randomised controlled study. *Lancet Neurol.* **6**, 765–772 (2007).
15. Ginzburg, L., Kacher, Y. & Futerman, A.H. The pathogenesis of glycosphingolipid storage disorders. *Semin. Cell Dev. Biol.* **15**, 417–431 (2004).
16. Jeyakumar, M., Dwek, R.A., Butters, T.D. & Platt, F.M. Storage solutions: treating lysosomal disorders of the brain. *Nat. Rev. Neurosci.* **6**, 713–725 (2005).
17. Christensen, K.A., Myers, J.T. & Swanson, J.A. pH-dependent regulation of lysosomal calcium in macrophages. *J. Cell Sci.* **115**, 599–607 (2002).
18. Bach, G., Chen, C.S. & Pagano, R.E. Elevated lysosomal pH in mucolipidosis type IV cells. *Clin. Chim. Acta* **280**, 173–179 (1999).
19. Parkesh, R. *et al.* Cell-permeant NAADP: A novel chemical tool enabling the study of Ca^{2+} signalling in intact cells. *Cell Calcium* **43**, 531–538 (2008).
20. Galione, A. & Churchill, G.C. Interactions between calcium release pathways: multiple messengers and multiple stores. *Cell Calcium* **32**, 343–354 (2002).
21. Churchill, G.C. *et al.* NAADP mobilizes Ca^{2+} from reserve granules, lysosome-related organelles, in sea urchin eggs. *Cell* **111**, 703–708 (2002).
22. Piper, R.C. & Luzio, J.P. CUPpling calcium to lysosomal biogenesis. *Trends Cell Biol.* **14**, 471–473 (2004).
23. Bilmen, J.G., Khan, S.Z., Javed, M.H. & Michelangeli, F. Inhibition of the SERCA Ca^{2+} pumps by curcumin. Curcumin putatively stabilizes the interaction between the nucleotide-binding and phosphorylation domains in the absence of ATP. *Eur. J. Biochem.* **268**, 6318–6327 (2001).
24. Infante, R.E. *et al.* Purified NPC1 protein: II. Localization of sterol binding to a 240–amino acid soluble luminal loop. *J. Biol. Chem.* **283**, 1064–1075 (2008).
25. Malathi, K. *et al.* Mutagenesis of the putative sterol-sensing domain of yeast Niemann Pick C–related protein reveals a primordial role in subcellular sphingolipid distribution. *J. Cell Biol.* **164**, 547–556 (2004).
26. Sun, X. *et al.* Niemann-Pick C variant detection by altered sphingolipid trafficking and correlation with mutations within a specific domain of NPC1. *Am. J. Hum. Genet.* **68**, 1361–1372 (2001).
27. Houben, E. *et al.* Differentiation-associated expression of ceramidase isoforms in cultured keratinocytes and epidermis. *J. Lipid Res.* **47**, 1063–1070 (2006).
28. Kagedal, K., Zhao, M., Svensson, I. & Brunk, U.T. Sphingosine-induced apoptosis is dependent on lysosomal proteases. *Biochem. J.* **359**, 335–343 (2001).
29. Kitatani, K., Idkowiak-Baldys, J. & Hannun, Y.A. The sphingolipid salvage pathway in ceramide metabolism and signaling. *Cell Signal.* **20**, 1010–1018 (2008).
30. Tettamanti, G., Bassi, R., Viani, P. & Riboni, L. Salvage pathways in glycosphingolipid metabolism. *Biochimie* **85**, 423–437 (2003).
31. Maceyka, M. *et al.* SphK1 and SphK2, sphingosine kinase isoenzymes with opposing functions in sphingolipid metabolism. *J. Biol. Chem.* **280**, 37118–37129 (2005).
32. Ozbay, T., Rowan, A., Leon, A., Patel, P. & Sewer, M.B. Cyclic adenosine 5′-monophosphate–dependent sphingosine-1-phosphate biosynthesis induces human *CYP17* gene transcription by activating cleavage of sterol regulatory element binding protein 1. *Endocrinology* **147**, 1427–1437 (2006).
33. Pandol, S.J., Schoeffield-Payne, M.S., Gukovskaya, A.S. & Rutherford, R.E. Sphingosine regulates Ca^{2+}-ATPase and reloading of intracellular Ca^{2+} stores in the pancreatic acinar cell. *Biochim. Biophys. Acta* **1195**, 45–50 (1994).
34. Walter, M., Chen, F.W., Tamari, F., Wang, R. & Ioannou, Y.A. Endosomal lipid accumulation in NPC1 leads to inhibition of PKC, hypophosphorylation of vimentin and Rab9 entrapment. *Biol. Cell* published online, doi:10.1042/BC20070171 (6 August 2008).
35. Garaschuk, O., Yaari, Y. & Konnerth, A. Release and sequestration of calcium by ryanodine-sensitive stores in rat hippocampal neurones. *J. Physiol. (Lond.)* **502**, 13–30 (1997).
36. Deisz, R.A., Meske, V., Treiber-Held, S., Albert, F. & Ohm, T.G. Pathological cholesterol metabolism fails to modify electrophysiological properties of afflicted neurones in Niemann-Pick disease type C. *Neuroscience* **130**, 867–873 (2005).
37. Lemons, R.M. & Thoene, J.G. Mediated calcium transport by isolated human fibroblast lysosomes. *J. Biol. Chem.* **266**, 14378–14382 (1991).
38. Srinivas, S.P., Ong, A., Goon, L., Goon, L. & Bonanno, J.A. Lysosomal Ca^{2+} stores in bovine corneal endothelium. *Invest. Ophthalmol. Vis. Sci.* **43**, 2341–2350 (2002).
39. Masson, M., Spezzatti, B., Chapman, J., Battisti, C. & Baumann, N. Calmodulin antagonists chlorpromazine and W-7 inhibit exogenous cholesterol esterification and sphingomyelinase activity in human skin fibroblast cultures. Similarities between drug-induced and Niemann-Pick type C lipidoses. *J. Neurosci. Res.* **31**, 84–88 (1992).
40. Mayran, N., Parton, R.G. & Gruenberg, J. Annexin II regulates multivesicular endosome biogenesis in the degradation pathway of animal cells. *EMBO J.* **22**, 3242–3253 (2003).
41. Ayala-Sanmartin, J., Henry, J.P. & Pradel, L.A. Cholesterol regulates membrane binding and aggregation by annexin 2 at submicromolar Ca^{2+} concentration. *Biochim. Biophys. Acta* **1510**, 18–28 (2001).
42. Wu, Y.P., Mizugishi, K., Bektas, M., Sandhoff, R. & Proia, R.L. Sphingosine kinase 1/S1P receptor signaling axis controls glial proliferation in mice with Sandhoff disease. *Hum. Mol. Genet.* **17**, 2257–2264 (2008).
43. Yamamoto, T. *et al.* Genotype-phenotype relationship of Niemann-Pick disease type C: a possible correlation between clinical onset and levels of NPC1 protein in isolated skin fibroblasts. *J. Med. Genet.* **37**, 707–712 (2000).
44. Pelled, D., Sperling, O. & Zoref-Shani, E. Abnormal purine and pyrimidine nucleotide content in primary astroglia cultures from hypoxanthine-guanine phosphoribosyltransferase–deficient transgenic mice. *J. Neurochem.* **72**, 1139–1145 (1999).
45. Rakovic, S. *et al.* An antagonist of cADP-ribose inhibits arrhythmogenic oscillations of intracellular Ca^{2+} in heart cells. *J. Biol. Chem.* **274**, 17820–17827 (1999).
46. He, X., Dagan, A., Gatt, S. & Schuchman, E.H. Simultaneous quantitative analysis of ceramide and sphingosine in mouse blood by naphthalene-2,3-dicarboxyaldehyde derivatization after hydrolysis with ceramidase. *Anal. Biochem.* **340**, 113–122 (2005).
47. Neville, D.C. *et al.* Analysis of fluorescently labeled glycosphingolipid-derived oligosaccharides following ceramide glycanase digestion and anthranilic acid labeling. *Anal. Biochem.* **331**, 275–282 (2004).
48. Yamaji, A. *et al.* Lysenin, a novel sphingomyelin-specific binding protein. *J. Biol. Chem.* **273**, 5300–5306 (1998).
49. Biwersi, J., Emans, N. & Verkman, A.S. Cystic fibrosis transmembrane conductance regulator activation stimulates endosome fusion in vivo. *Proc. Natl. Acad. Sci. USA* **93**, 12484–12489 (1996).
50. Elliot-Smith, E. *et al.* Beneficial effects of substrate reduction therapy in a mouse model of GM1 gangliosidosis. *Mol. Genet. Metab.* **94**, 204–211 (2008).